Ibn Al-Haitham Journal for Pure and Applied Sciences
Journal homepage: jih.uobaghdad.edu.iq
PISSN: 1609-4042, EISSN: 2521-3407
IHJPAS. 2026; 39(1)

2D Photocatalyst System of Mn_3O_4: Ag Nanocomposite to the Degradation of Methylene Blue Under Solar Light

Rawaa H. Salman[1], Lekaa K. Abdul Karem[2*], and Ahmed M. Khalil[3]
[1,2] Department of Chemistry, College of Education for Pure Science (Ibn Al-Haitham), University of Baghdad, Baghdad, Iraq
[3]Photochemistry Department, National Research Centre, 33 El-Bohouth St, Dokki, Giza, 12622, Egypt
*Corresponding Author

Received: 23/May/2025
Accepted: 24/August/2025
Published: 20/ January /2026
doi.org/10.30526/39.1.4209

Abstract

Constructing two-dimensional (2D) composites using layered materials is considered a practical approach to achieving high-efficiency photocatalysts. This study aims to prepare manganese oxide nanoparticles (NPs) from the aqueous extract of thyme leaves, characterize them by spectroscopic methods, and bridge the gap by developing an environmentally friendly, photostable coating and evaluating its efficiency in degrading the methylene blue (MB) dye under sunlight, suitable for practical water treatment applications. In this work, a 2D nano-photocatalytic coating of Mn_3O_4:Ag was developed for the efficient removal of organics and pollutants from water under sunlight. The method involves synthesizing a photocatalytic nanomaterial via green synthesis of a Mn_3O_4/Ag nanocomposite using thyme leaf extract. The products were characterized using X-ray diffraction, Fourier transform infrared spectroscopy, and scanning electron microscopy. The image of the Mn_3O_4: Ag nanocomposite showed spherical NPs with extensive aggregation. The average crystal size was calculated to be 23.7 nm using the Debye-Scherrer equation, and the crystals were incorporated into a white, waterproof coating to produce a homogeneous nano-coating. The final product is applied to solid surfaces and dried at room temperature. The resulting layer demonstrates high efficiency in degrading the MB dye, a model pollutant. The system is eco-friendly, cost-effective, and suitable for water treatment applications. The advantage of this work is the use of green synthesis to produce Mn_3O_4:Ag nanocomposite, which is incorporated into a coating that serves as a photocatalytic layer under sunlight, making it suitable for environmental remediation applications.

Keywords: Mn_3O_4:Ag Nanocomposite, Photocatalysis, Two-dimensional, Water treatment.

1. Introduction

Water contamination from industrial discharges, including dyes such as MB, continues to threaten ecosystems and human health. Effective treatment and reuse of wastewater are essential for ensuring environmental protection and sustainable development[1]. Industrial expansion, especially in textiles, has led to the continuous discharge of hazardous substances into aquatic systems. These pollutants pose significant risks due to their persistence and toxicity[2]. Conventional treatment methods, such as chemical precipitation and biological degradation, often prove ineffective at entirely removing complex organic pollutants[3]. Various treatment strategies have been adopted to address pollution-related issues. Recent studies have increasingly focused on advanced oxidation processes (AOPs). Among these, photocatalysis stands out for its efficiency, low cost, and eco-friendliness, making it one of the most widely used AOP

techniques in water treatment. Semiconductor photocatalysts have attracted significant attention for innovative physicochemical methods due to their low energy requirements and simplicity[4,5]. This process relies on the excitation of electrons from the semiconductor's valence band to the conduction band, leaving behind holes. These electron–hole pairs initiate redox reactions that generate reactive oxygen species (ROS), which then degrade organic pollutants[6,7]. Among various semiconductors, manganese oxide (Mn_3O_4) has received considerable interest due to its favorable redox behavior, mixed valence states (Mn^{2+}: Mn^{3+}), spinel structure, and efficient catalytic activity under light[8-10]. Mn_3O_4-based photocatalysts encounter a substantial constraint stemming from the swift recombination of photogenerated electron–hole pairs, which markedly diminishes their photocatalytic effectiveness. To resolve this issue, researchers have investigated the incorporation of noble metals, such as silver (Ag), with Mn_3O_4 to enhance charge separation and extend the longevity of photogenerated carriers[11-13]. However, using suspended photocatalysts presents practical limitations, including difficulty in recovery, limited reuse, and secondary pollution. To address this, researchers have focused on immobilizing nanocatalysts onto solid substrates via coatings or films, enabling fixed-bed photocatalytic systems[14]. Nanostructured coatings offer several advantages, including mechanical stability, chemical resistance, improved durability, and the ability to provide additional functional properties, such as UV protection, antimicrobial effects, and self-cleaning behavior. These features make them ideal for environmental, electronic, and industrial applications[15]. Industrial coatings based on organic–inorganic hybrids, particularly those synthesized via sol-gel processes, have emerged as advanced solutions due to their customizable chemical and mechanical properties. These coatings combine hardness, durability, and flexibility[16]. Various synthesis routes have been developed to fabricate such nanostructured coatings, ranging from traditional vapor deposition to modern methods such as sol–gel and laser cladding[17,18]. Despite these advancements, the green synthesis and immobilization of Mn_3O_4:Ag nanocomposites in water-repellent coatings remain underexplored. This study aims to prepare manganese oxide nanoparticles (NPs) from the aqueous extract of thyme leaves and characterize them by spectroscopic methods. The study also aimed to bridge the gap by developing an environmentally friendly, photostable coating and evaluating its efficiency in degrading the methylene blue (MB) dye under sunlight, suitable for practical water treatment applications.

2. Materials and Methods

Silver nitrate ($AgNO_3$) was procured from Merck (Germany), manganese (II) sulfate monohydrate ($MnSO_4 \cdot H_2O$) from Qualikems (India), deionized water (DI water), and Thymus vulgaris leaves. The rubber coating was commercially obtained from a local supplier. A plastic container with dimensions of (20 x 20) cm was used as the coating bath.

2.1. Preparation of the photocatalytic coating

The Mn_3O_4:Ag nano composite used in this study was synthesized by mixing two individually prepared silver NPs (Ag NPs) and manganese oxide NPs. Both NPs were green-synthesized using plant extract. The selected weight ratio of Mn_3O_4 to Ag was 1:0.5, ensuring uniform dispersion and optimal integration of both components. Each NP was dispersed in deionized water, and the resulting suspensions were combined and ultrasonicated. The green synthesis of Mn_3O_4:Ag nanocoating for photocatalytic applications is shown in **Figure 1**. The mixture was subjected to thermal condensation and then dried at 80°C. To prepare the photocatalytic coating, different amounts of the three (1%, 2%, and 4% w/w) were manually blended with a liquid white dye to form a solid-in-liquid dispersion. The mixture was stirred by hand, and the resulting formulations were applied directly to the inner surface of a clean plastic basin using a brush, forming a thin, even film.

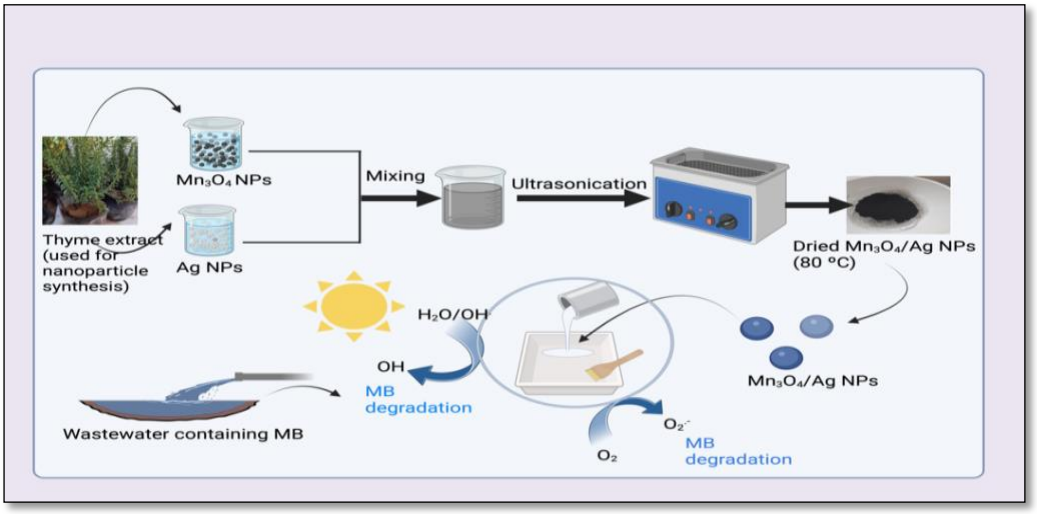

Figure 1. Green synthesis of Mn_3O_4:Ag nanocoating for photocatalytic application**.**

After coating, it was left to dry at room temperature overnight to allow complete evaporation of the liquid phase. The thoroughly dried coating was then used for photocatalytic degradation experiments under sunlight[19].

2.1.1. Photocatalytic degradation procedure

The photocatalytic efficiency of the coated plastic basin was evaluated by the degradation of a white dye under natural sunlight. A stock solution of MB was prepared at 1000 ppm by dissolving the required amount of dye powder in deionized water. From this stock, a 200 ppm solution was prepared by diluting 40 mL of the stock with 160 mL of deionized water to a final volume of 200 mL. The nanocomposite was incorporated into a waterproof, white, rubber-based dye, which was applied to the inner surface of the plastic basin using a brush. The coating was left to dry overnight at room temperature, forming a water-resistant photocatalytic film. The system was exposed to direct sunlight for 72 hours. Aliquots were withdrawn and analyzed using a UV-Vis spectrophotometer. The maximum absorption wavelength (λ_{max}) of MB was determined to be 664 nm, and all measurements were performed at this wavelength to monitor degradation[20]. The degradation efficiency (R%) was calculated using the following **Equation 1**:

$$R\% = (c_0 - c_t \backslash c_0) \times 100 \quad \textbf{(1)}$$

Where: C_0 is the initial dye concentration, and C_t is the dye concentration at time

Based on the Beer–Lambert Law, which assumes a linear correlation between absorbance and concentration, C_t values were estimated from absorbance readings as **Equation 2**:

$$R\% = (A_0 - A_t / A_0) \times 100 \quad \textbf{(2)}$$

Where A_0 and A_t are the absorbance values at the initial time and time t, respectively, the average solar irradiance recorded during the exposure period was 900 W/m².

2.1.2. Product characterization

The compounds were synthesized and characterized utilizing diverse spectroscopic and microscopic methodologies and apparatus, including a magnetic stirrer, a PC21-A electric oven, a Batec, and a PLC (80-1) electric centrifuge. A sensitive electronic balance (AS 220C1) was utilized for accurate measurements. X-ray diffraction (XRD) investigation was conducted utilizing a Phillips PW1730 from the Netherlands. The FT-IR spectra were acquired using a Shimadzu 1800 (Japan) over 400-4000 cm^{-1}, and field-emission scanning electron microscopy (FESEM) was performed using a MIRA II (Czech Republic). The colors of the treated and untreated samples were determined using a ColorFlex spectrophotometer in accordance with ASTM E313-10. The samples with thick plaques (2 mm) and flattened surfaces were placed in the specimen measuring port, and L* was monitored.

3.Results

3.1. FTIR spectrum characterization

The FTIR spectrum that is shown in **Figure 2** exhibited Mn–O stretching bands at (500, 700, and 915) cm^{-1}, indicative of Mn–O stretching vibrations. The spectrum appeared bands at (3441, 3194, 2936, 1734, and 1652) cm^{-1}.

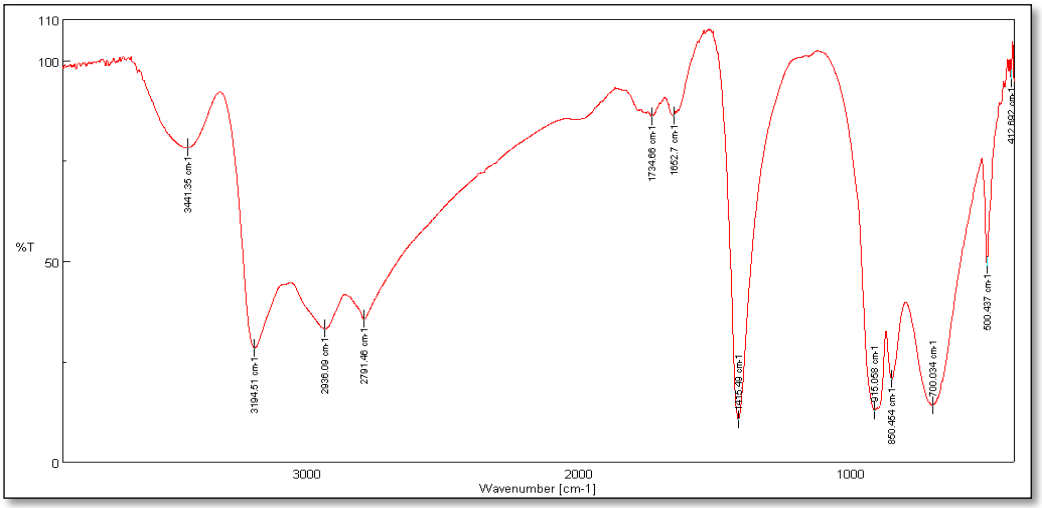

Figure 2. FTIR spectrum of the Mn_3O_4:Ag nanocomposite

3.2. XRD pattern of the produced Mn_3O_4/Ag nanocomposite

The XRD pattern of the produced Mn_3O_4:Ag nanocomposite is presented in **Figure 3** and **Table 1**. The diffract gram shows distinct peaks at 2θ = 33.4°, 38.6°, 44.7°, 55.6°, 64.9°, and 77.8°.

Table 1. XRD data of the Mn_3O_4:Ag nanocomposite.

No.	2θº	hkl	FWHM (degree)	2θº (Rad.)	FWHM (Rad)	D (nm)
1	33.4	320	0.2362	0.291558	0.004	35.108
2	38.6	111	0.3306	0.336437	0.006	25.445
3	44.7	200	0.6612	0.390448	0.012	12.987
4	55.6	051	0.3306	0.48505	0.006	27.151
5	64.9	220	0.4723	0.565935	0.008	19.919
6	77.8	220	0.4723	0.678907	0.008	21.604

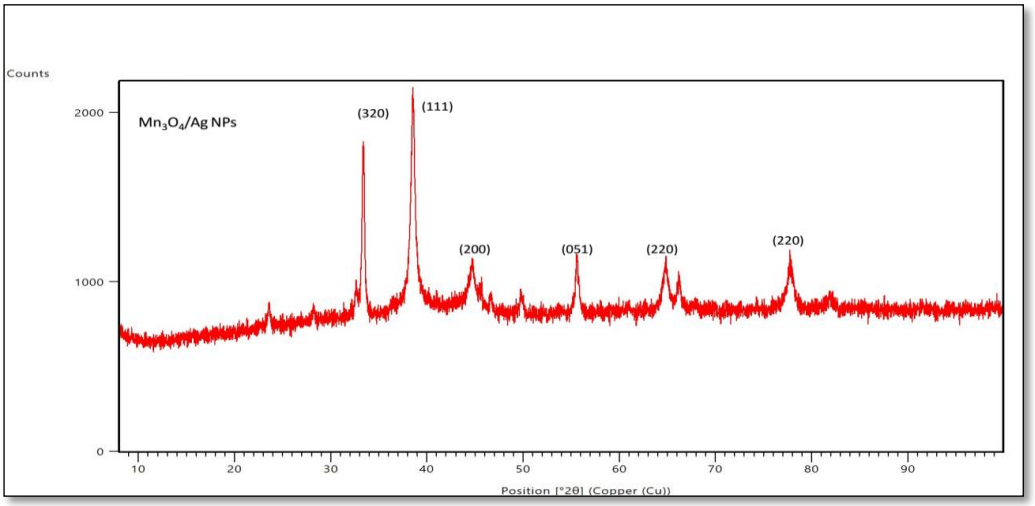

Figure 3. XRD picture of the Mn_3O_4:Ag nanocomposite

3.3.FESEM of the Mn_3O_4:Ag

FESEM picture of the Mn_3O_4:Ag nanocomposite, **Figure 4** illustrating quasi-spherical NPs with significant aggregation. The particle sizes ranged from 30 to 80 nm, confirming the material's nanoscale nature.

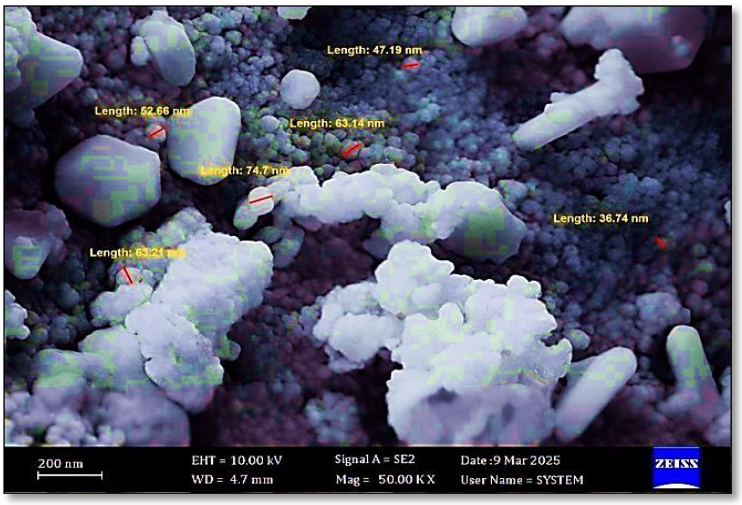

Figure 4. FESEM pictures of the Mn_3O_4:Ag nanocomposite

3.4. Photocatalytic degradation of MB

Photocatalytic degradation behavior of MB under sunlight in the presence of Mn_3O_4:Ag-based coatings with different catalyst loadings (1%, 2%, and 4% w/w), as shown in **Figure 5**.

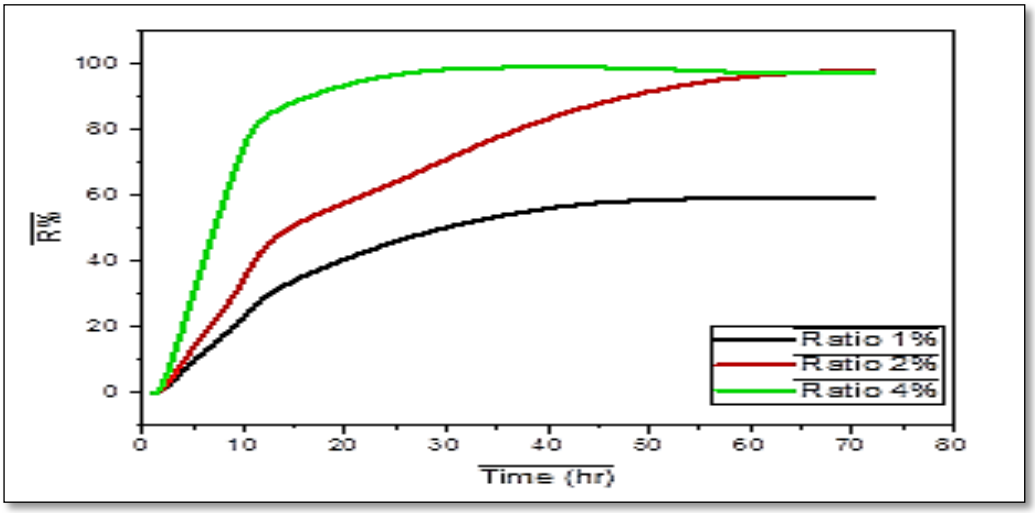

Figure 5. The R% of MB using coated films with Mn_3O_4: Ag-coated films (1, 2, and 4)%

The absorbance of the dye solution gradually decreased with increasing exposure time, indicating continuous degradation. The 2% Mn_3O_4:Ag coating demonstrated the most efficient dye removal, with the absorbance curve showing a sharp decline and stabilizing after 72 hours. The 4% coating presented a high performance, although slightly lower than the 2%, while the 1% formulation exhibited the slowest and least effective degradation.

3.5. Colorimetric evaluation

Colorimetric analysis was conducted to evaluate the lightness (L*) of the Mn_3O_4:Ag-based coatings before sunlight exposure. As shown by the measurements, the 1% formulation exhibited the highest L* value (85.49), indicating a closer match to the original white dye. Increasing the catalyst concentration led to darker initial coatings, with L* values of 73.58 and 70.74 for 2% and 4% catalyst loadings, respectively. These results suggest that higher nanocomposite content

reduces the coating's optical brightness at the outset and present the complete colorimetric data for the coated samples before sunlight exposure. While various parameters were measured (such as a*, b*, and ΔE), the current analysis focuses solely on L*, which indicates the surface's visual lightness. The corresponding visual color distributions are shown in **Figure 6**, highlighting differences in sample appearance across loadings.

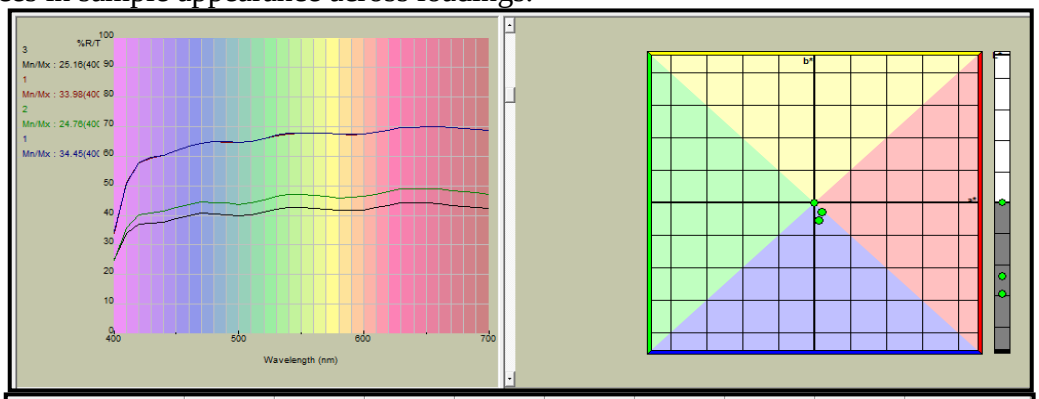

ID	L*	a*	b*	dL*	da*	db*	dE*	dE CMC	dE CMC (l:c)
1	85.50	0.57-	4.81	85.50	0.57-	4.81			
+Tolerances	0.00	0.00	0.00	0.00	0.00	0.00	0.00	1.00	
-Tolerances	0.00	0.00	0.00	0.00	0.00	0.00	0.00	1.00	
2	73.58	0.14-	4.21	11.92-	0.42	0.60-	11.94	4.35	2.00 : 1.00
1	85.49	0.57-	4.77	0.01-	0.01-	0.03-	0.04	0.04	2.00 : 1.00
3	70.74	0.29-	3.72	14.76-	0.28	1.09-	14.80	5.42	2.00 : 1.00

Figure 6. Color space representation and spectral reflectance curve of Mn_3O_4:Ag-coated samples

4. Discussion

4.1. FTIR spectrum

The FTIR spectrum in **Figure 2** shows bands at 500, 700, and 915 cm^{-1}, indicative of Mn–O stretching vibrations, confirming the formation of Mn_3O_4. The other bands, which appear at (3441, 3194, 2936, 1734, and 1652) cm^{-1}, refer to stretching vibration of O-H, N-H, C-H aliphatic groups, C=O, and C=C, respectively, originating from residual phytochemicals present in plant extract used during green synthesis[20-22].

4.2. XRD pattern

The observed peaks in **Figure 3** and **Table 1** correspond to the crystallographic planes (hkl) of Mn_3O_4 and Ag phases, consistent with JCPDS card no. 01-086-2337 and JCPDS no. 01-087-0719, respectively. The pronounced peak at 38.6°, associated with the (111) plane, verifies the existence of face-centered cubic silver NPs[23]. The crystallite size was determined using the Debye–Scherrer equation ($D= K\lambda/\beta\cos\theta$). The average crystallite size measured 23.7 nm, affirming the nanoscale architecture of the produced material. The absence of any additional distinct peaks indicates that the synthesized Mn_3O_4:Ag nanocomposite is highly crystalline, confirming the structural purity of the material. These characteristic peaks validate the successful synthesis of the nanocomposite[20].

4.3. FESEM

This partial agglomeration is frequently reported in green-synthesized nanomaterials. This agglomeration is due to two factors, primarily attributed to the high surface energy of the nanoscale particles, which drives them to coalesce to minimize surface tension. Additionally, the absence of a chemical stabilizer in the green synthesis method reduces electrostatic repulsion between particles, further promoting aggregation. Nevertheless, this structural clustering does not compromise the crystalline purity of the nanocomposite, as confirmed by the XRD and FTIR analyses. The particle surfaces were not completely smooth; instead, they exhibited nanoscale imperfections and tiny granular features, as shown in **Figure 4**. Surface asperities can increase the effective surface area and facilitate interactions with surrounding media, which is advantageous in surface-dependent applications, including photocatalysis[22].

4.4. Photocatalytic degradation of MB

The results suggest that increasing the catalyst loading improves the photocatalytic activity up to an optimal point. The 2% loading achieved the highest degradation efficiency (98% within 72 hours), indicating sufficient surface area and active sites without excessive particle agglomeration. In contrast, the 1% catalyst may have had insufficient active centers, while the 4% catalyst may have led to excess coverage or light scattering, slightly reducing performance. Therefore, 2% catalyst loading provides the most balanced and effective degradation behavior under sunlight irradiation[22], as shown in **Figure 5**.

4.5. Colorimetric evaluation of Mn_3O_4:Ag NPs

The observed decrease in L* values with increasing catalyst concentration suggests that the Mn_3O_4:Ag nanocomposite layer becomes optically darker at higher loadings. This may be due to greater surface coverage, higher particle density, or increased light absorption caused by the dense nanostructure. A lower L* value at 2% and 4% loading could also indicate enhanced light interaction, which may benefit photocatalytic efficiency. Therefore, the colorimetric differences reflect structural and optical changes in the coating as a function of catalyst concentration. Optimizing catalyst loading is essential for attaining a functioning photocatalytic coating that provides both high degrading efficiency and satisfactory visual characteristics. The 1% Mn_3O_4:Ag coating demonstrated the highest lightness value (L*= 85.49), signifying negligible visible disruption to the original white dye. Nonetheless, it yielded the lowest photocatalytic efficiency (59%). The 2% formulation demonstrated exceptional photocatalytic performance (98%) and sustained a relatively high L* value (73.58), indicating a favorable equilibrium between catalytic efficacy and surface aesthetics. In contrast, the 4% loading attained a similar deterioration (97%) but exhibited increased darkening (L*= 70.74), potentially diminishing its visual appeal. The 2% catalyst loading was identified as the best composition, yielding effective dye degradation and satisfactory visual stability, thereby positioning it as a viable contender for practical applications[23].

5. Conclusion

This study demonstrated that Mn_3O_4:Ag-based photocatalytic coatings prepared with a rubber-based white dye were effective in degrading MB under sunlight. Including the tested formulations, the 2% catalyst loading achieved the highest degradation efficiency (98%) within 72 hours while also maintaining acceptable visual properties (L*= 73.58). Although the 1% composition exhibited better lightness, it showed limited photocatalytic performance. Therefore, the 2% formulation was identified as the optimal balance between functionality and appearance, making it a promising candidate for practical photocatalytic applications involving surface coatings. A distinctive green-synthesized Mn_3O_4/Ag nanocomposite is presented for solar-driven degradation of organic dyes, addressing a direction that remains underexplored in the current literature.

Acknowledgment

The authors thank the Department of Chemistry, College of Education for Pure Science (Ibn Al-Haitham) for their support in completing this research.

Conflict of Interest

The authors declare that they have no conflicts of interest.

Funding

There is no funding for this study.

References

1. Najjar EH, Kianfar AH, Dinari M, Rezaei B, Saeidi S. Photocatalytic activity of the novel triazine-based magnetic core–shell Cu nanocomposite for degradation of RhB and MB via air oxidation and Cr (VI) reduction. Environ. Nanotechnol Monit Manag. 2023; 20:100820. https://doi.org/10.1016/j.enmm.2023.100820.
2. Byeon H, Sunil J. Dye degradation, pathogen control, photocatalytic and antibacterial phenomena of green-synthesized ZnO-polypyrrole nanocomposites. J Mol Liq. 2025; 430(1):127683. https://doi.org/10.1016/j.molliq.2025.127683.
3. Yadav D, Sharma N, Sharma P, Preeti, Das A, Rawat P, Majumder S, Srivastava CM. Synergistic photocatalytic degradation of multiple class of organic pollutants using GO-TiO_2-WO_3 nanocomposite. Mater Sci Eng B. 2025; 317(2-3):118241. https://doi.org/10.1016/j.mseb.2025.118241.
4. Matei E, Ștăulean AA, Râpă M, Constandache A, Predescu AM, Coman G, Berbecaru AC, Predescu C. ZnO nanostructured matrix as nexus catalysts for the removal of emerging pollutants. Environ Sci Pollut Res. 2023; 30(54):114779-114821. https://doi.org/10.1007/s11356-023-30713-3.
5. Ramalingam G, Perumal N, Priya AK, Rajendran S. A review of graphene-based semiconductors for photocatalytic degradation of pollutants in wastewater. Chemosphere. 2022; 300:134391. https://doi.org/10.1016/j.chemosphere.2022.134391.
6. Atacan K, Güy N, Özacar M. Recent advances in photocatalytic coatings for antimicrobial surfaces. Curr Opin Chem Eng. 2022; 36:100777. https://doi.org/10.1016/j.coche.2021.100777.
7. Anjaneyulu B, Chauhan V, Chinmay, Afshari M. Enhancing photocatalytic wastewater treatment: investigating the promising applications of nickel ferrite and its novel nanocomposites. Environ Sci Pollut Res. 2024; 31(31):43453-43475. https://doi.org/10.1007/s11356-024-33502-8.
8. Magesh G, Arun AP, Poonguzhali RV, Kumar ER, Pradeep I, Kumar RR, Abd El-Rehim AF. Pure α-MnO_2 and Ag decorated α-MnO_2 nanorods for photocatalytic activity. J Mol Struct. 2025; 1329:141444. https://doi.org/10.1016/j.molstruc.2025.141444.
9. Chen P, Zhu Y, Ge T, Castell MR. Scanning tunneling microscopy of MnOx ultrathin films on Au (111). Surf Sci. 2023; 730:122248. https://doi.org/10.1016/j.susc.2023.122248.
10. Annese E, Alí A, Barreto J, Felix G, Stavale F. Unraveling hausmannite (Mn_3O_4) thin films surface structure by X ray linear dichroism. Appl Surf Sci. 2022; 578:151944. https://doi.org/10.1016/j.apsusc.2021.151944.
11. Uddin J, Abdur R, Hossain MR, Aziz S, Jamal MS, Shaikh MA, Hossain M. Phase tunable nickel doped Mn_3O_4 nanoparticle synthesis by chemical precipitation: Kinetic study on dye degradation. Nanoscale Adv. 2024; 6(3):902-909. https://doi.org/10.1039/D3NA00754E.
12. Rizal MY, Saleh R, Prakoso SP, Taufik A, Yin S. Ultraviolet-and visible-light photocatalytic and sonophotocatalytic activities toward Congo red degradation using Ag/ Mn_3O_4 nanocomposites. Mat Sci Semicon Proc. 2021; 121:105371. https://doi.org/10.1016/j.mssp.2020.105371.
13. Frederichi D, Scaliante MHN, Bergamasco R. Structured photocatalytic systems: photocatalytic coatings on low-cost structures for treatment of water contaminated with micropollutants—a short review. Environ. Sci. Pollut. Res. 2021; 28(19):23610-23633. https://doi.org/10.1007/s11356-020-10022-9.
14. Farooq SA, Raina A, Mohan S, Singh RA, Jayalakshmi S, Irfan Ul Haq M. Nanostructured coatings: Review on processing techniques, corrosion behaviour and tribological performance. Nanomaterials. 2022; 12(8):1323. https://doi.org/10.3390/nano12081323.
15. Ielo I, Giacobello F, Sfameni S, Rando G, Galletta M, Trovato V, Rosace G, Plutino MR. Nanostructured surface finishing and coatings: Functional properties and applications. Materials. 2021; 14(11):2733. https://doi.org/10.3390/ma14112733.
16. Adak D, Bhattacharyya R, Barshilia HC. A state-of-the-art review on the multifunctional self-cleaning nanostructured coatings for PV panels, CSP mirrors and related solar devices. Renew Sustain Energy Rev. 2022; 159:112145. https://doi.org/10.1016/j.rser.2022.112145.
17. Ma J, Xiao Y, Chen J, Shen Y, Xiao S, Cao S. Dual-pathway charge transfer mechanism of anatase/rutile TiO_2-Ag_3PO_4 hollow photocatalyst promotes efficient degradation of pesticides. J Colloid Interface Sci. 2025; 678(Part A):334-344. https://doi.org/10.1016/j.jcis.2024.08.162.

18. Khan S, Hussain A, He K, Liu B, Imran Z, Ambreen J, Hassan S, Ahmad M, Batool SS, Li C. Tailoring the bandgap of Mn_3O_4 for visible light driven photocatalysis. J Environ Manage. 2021; 293: 112854. https://doi.org/10.1016/j.jenvman.2021.112854.
19. Osgouei MS, Khatamian M, Kakili H. Improved visible-light photocatalytic activity of Mn_3O_4-based nanocomposites in removal of methyl orange. Mater Chem Phys. 2020; 239:122108. https://doi.org/10.1016/j.matchemphys.2019.122108.
20. Hussain S, Aslam A, Tajammal A, Othman F, Mustafa Z, Alsuhaibani AM, Refat MS, Shahid M, Sagir M, Zakaria ZA. Tagetes erecta-mediated biosynthesis of Mn_3O_4 nanoparticles: Structural, electrochemical, and biological investigations. ACS Oamega. 2024; 9(33):35408-35419. https://doi.org/10.1021/acsomega.4c01328.
21. Radhi IM, Abd SS, Faraj RAS, Abbas AM, Himdan TA. A using activated and modified adsorbent surfaces from banana peels to remove the green Janus dye: A kinetic, isothermal, and thermodynamic study. Mong J Chem. 2024; 25(52):19-25. https://doi.org/10.5564/mjc.v25i52.3450.
22. Khalil AS, Al-Shabander BM, Yaseen HM. Photocatalytic activity of tetragonal $BaTiO_3$ nanoparticles prepared by wet chemical method. In AIP Conference Proceedings. 2021; 2372(1):130019. https://doi.org/10.1063/5.0066068.
23. Jawad AH, Sabar S, Ishak MA, Wilson LD, Ahmad Norrahma SS, Talari MK, Farhan AM. Microwave-assisted preparation of mesoporous-activated carbon from coconut (Cocos nucifera) leaf by H_3PO_4 activation for methylene blue adsorption. Chem Eng Commun. 2017; 204(10):1143-1156. https://doi.org/10.1080/00986445.2017.1347565.